A Physics-Based Analytical Model for Perovskite Solar Cells

Xingshu Sun, *Student Member, IEEE*, Reza Asadpour, Wanyi Nie, Aditya D. Mohite,
and Muhammad Ashraful Alam, *Fellow, IEEE*

Abstract—Perovskites are promising next-generation absorber materials for low-cost and high-efficiency solar cells. Although perovskite cells are configured similar to the classical solar cells, their operation is unique and requires development of a new physical model for characterization, optimization of the cells, and prediction of the panel performance. In this paper, we develop such a physics-based analytical model to describe the operation of different types of perovskite solar cells, explicitly accounting for nonuniform generation, carrier selective transport layers, and voltage-dependent carrier collection. The model would allow experimentalists to characterize key parameters of existing cells, understand performance bottlenecks, and predict performance of perovskite-based solar panel—the obvious next step to the evolution of perovskite solar cell technology.

Index Terms—Analytical model, characterization, drift-diffusion, panel simulation.

I. INTRODUCTION

SOLAR cells have emerged as an important source of renewable energy; further reduction in cost will ensure a broader and accelerated adoption. Recently, organic–inorganic hybrid perovskites, such as $CH_3NH_3PbI_3$, have shown great promise as new absorber materials for low-cost highly efficient solar cells [1]–[3]. Despite a growing literature on the topic, most of theoretical work to date has been empirical or fully numerical [4]–[8]. The detailed numerical models provide deep insights into the operation of the cells and its fundamental performance bottlenecks, but are generally unsuitable for fast characterization, screening, and/or prediction of panel performance. Indeed, the field still lacks an intuitively simple physics-based analytical model that can interpret the essence of device operation with relatively few parameters, which can be used to characterize, screen, and optimize perovskite-based solar cells; provide preliminary results for more sophisticated device simulation; and allow panel-level simulation for perovskites. This state-of-the-art reflects the fact that despite a superficial similarity with p-n [9]–[11] or p-i-n [12]–[14] solar cells, the structure,
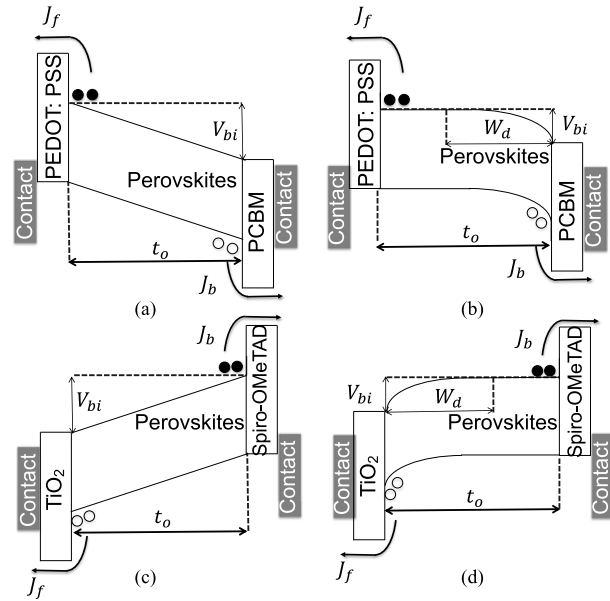
Fig. 1. Energy diagram of perovskite solar cells in traditional structure (PEDOT:PSS/Perovskite/PCBM). (a) Type-1 (p-i-n) and (b) Type-2 (p-p-n) and titania-based inverted cells (TiO$_2$/Perovskite/Spiro-OMeTAD). (c) Type-3 (n-i-p) and (d) Type-4 (n-p-p).

self-doping, and charge collection in perovskite cells are unique and cannot described by traditional approaches [15], [16].

In this paper, we present a new physics-based analytical model that captures the essential features of perovskite cells, namely, position-dependent photogeneration, the role of carrier transport layers, e.g., TiO$_2$ and Spiro-OMeTAD, in blocking charge loss at wrong contacts, voltage-dependent carrier collection that depends on the degree of self-doping of the absorber layer, etc. The model is systematically validated against the four classes of perovskite solar cells reported in the literature. We demonstrate how the model can be used to obtain physical parameters of a cell and how the efficiency can be improved. Our model can be easily converted into a physics-based equivalent circuit that is essential for accurate and complex large-scale network simulation to evaluate and optimize perovskite-based solar modules and panels [13], [17]–[20].

II. MODEL DEVELOPMENT AND VALIDATION

A typical cell consists of a perovskite absorber layer (300–500 nm), a hole transport layer (p-type), an electron transport layer (n-type), and front and back contacts, arranged in various configurations. The traditional structure in Fig. 1(a) and (b) has PEDOT:PSS and PCBM as the front hole transport layer

and the back electron transport layer, respectively; in the inverted structure, however, TiO_2 is the front electron transport layer and Spiro-OMeTAD is the back hole transport layer, as in Fig. 1(c) and (d). Moreover, for both the traditional and inverted configurations, it has been argued that the absorber layer in high-efficiency cells is essentially intrinsic [21] [see Fig. 1(a) and (c)]; the mode of operation changes and the efficiency is reduced for cells with significant p-type self-doping [22] [see Fig. 1(b) and (d)]. Therefore, perovskite solar cells can be grouped into (Type-1) p-i-n, (Type-2) p-p-n, (Type-3) n-i-p, and (Type-4) n-p-p cells; the corresponding energy band diagrams are shown in Fig. 1.

It has been suggested that the high dielectric constant of perovskites allows the photogenerated excitons to dissociate immediately into free carriers [23], [24]. The photogenerated electron and holes then drift and diffuse through the absorber and transport layers before being collected by the contacts. Consequently, an analytical model can be developed by solving the steady-state electron and hole continuity equations within the absorber, namely

$$D\frac{\partial^2 n(x)}{\partial x^2} + \mu E(x)\frac{\partial n(x)}{\partial x} + G(x) - R(x) = 0 \quad (1)$$

$$D\frac{\partial^2 p(x)}{\partial x^2} - \mu E(x)\frac{\partial p(x)}{\partial x} + G(x) - R(x) = 0. \quad (2)$$

Here, $n(p)$ is the electron/hole concentration, D and μ are the diffusion coefficient and mobility, respectively, and $G(x)$ represents the position-dependent photogeneration. The extraordinarily long diffusion length in perovskite [25]–[27] ensures that one can ignore carrier recombination within the absorber layer, i.e., $R(x) = 0$. Finally, $E(x)$ is the position-resolved electric field within the absorber layer.

As shown in Fig. 1, $E(x)$ is a constant (linear potential profile) for type-1 (n-i-p) and type-3 (p-i-n) cells, i.e., the absence of doping or trapped charges ensure that $E(x) = (V_{bi} - V)/t_0$, where V_{bi} is the build-in potential, and t_0 is the thickness of the intrinsic layer. For type-2 (p-p-n) and type-4 (n-p-p) devices, however, numerical simulation shows that the field is essentially linear within the depletion region, i.e., $E(x) = [1 - x/W_d] E_{max}(V)$, where W_d is the depletion width, and $|E_{max}(V)| = 2(V_{bi} - V)/W_d(V)$; $E(x) = 0$ in the neutral region defined by $x > W_d$. The position-dependent $E(x)$ is reflected in the parabolic potential profiles shown in Fig. 1(b) and (d). Our extensive numerical simulation [21] shows that the photogenerated carriers do not perturb the electric field significantly; therefore, the following analysis will presume $E(x)$ is independent of photogeneration at 1-sun illumination.

Neglecting any parasitic reflectance from the back surface, we approximate the generated profile in the absorber layer as $G(x) = G_{eff} e^{-x/\lambda_{ave}}$, where G_{eff} and λ_{ave} ($\sim$100 nm) are the material specific constants, averaged over the solar spectrum. Note that the maximum absorption is

$$G_{max} = \int_0^\infty G_{eff} e^{-x/\lambda_{ave}} dx = G_{eff}\lambda_{ave}.$$

Finally, electron and hole transport layers are considered perfect conductors for the majority carriers, while they act as imperfect blocking layers for the minority carriers, characterized by the effective surface recombination velocity $|J_{f(b)}| = qs_{f(b)}\Delta n(p)$. The $\Delta n(p)$ is the excess minority carrier concentration, and the $s_{f(b)}$ is the effective surface recombination velocity at the front (back) transport layer, accounting for three recombination processes: 1) carrier escape at the wrong contact; 2) recombination due to the interface defects; and 3) recombination within the bulk of the transport layer.

Remarkably, (1) and (2) can be solved analytically to derive the complete current–voltage characteristics of the four types of perovskite cells, as follows:

$$J_{dark} = (\alpha_f \times J_{f0} + \alpha_b \times J_{b0})\left(e^{\frac{qV}{kT}} - 1\right) \quad (3)$$

$$J_{photo} = qG_{max}(A - Be^{-m}) \quad (4)$$

$$J_{light} = J_{dark} + J_{photo}. \quad (5)$$

The parameters of the model, namely, $\alpha_{f(b)}, \beta_{f(b)}, A(B), m, n,$ and Δ are functions of the following physical parameters of the cell (see Table I): t_0 is the thickness of the absorber layer, $J_{f0(b0)}$ is the dark diode current recombining at the front/back transport layer, V_{bi} is the built-in potential across the absorber layer, D is the diffusion coefficient, $s_{f(b)}$ is the effective surface recombination velocity at the front/back interface, $W_d(0V)$ is the equilibrium depletion width for self-doped devices, and G_{max} is the maximum absorption.

Among these parameters, G_{max} is obtained by integrating the position-dependent photon absorption calculated by the transfer matrix method [28] (here, $qG_{max} = 23$ mA/cm^2), $D \approx 0.05$ cm$^2 \cdot$ s^{-1} is known for the material system for both electron and hole [26], and V_{bi} can be estimated either by using the capacitance–voltage characteristics [22] or by using the crossover voltage of the dark and light I–V [29]. The effective surface recombination velocities can be fitted using the photogenerated current $J_{photo}(G, V) = J_{light}(G, V) - J_{dark}(V)$ [30]. Finally, we can obtain the dark diode current $J_{f0/b0}$ by fitting the dark current.

In order to validate the model, we fit both dark and light I–V characteristics for four different perovskite cells using the model as shown in Fig. 2. See the Appendix for the details of the fitting algorithm. Samples #1 (15.7%) and #2 (11.1%) are solution-based PCBM-based architecture (Type-1 and Type-2) [21], whereas samples #3 (15.4%) and #4 (8.6%) are titania-based inverted architecture (Type-3 and Type-4) fabricated by vapor deposition and solution processes, respectively [31]. The fitting parameters obtained for the four samples are summarized in Table II. Remarkably, the analytical model not only reproduces the key features of the I–V characteristics of very different cell geometries, but also captures very well the known physical parameters of the cell (e.g., thickness of the absorber). Indeed, the error in the power output due to imperfect fitting is less than 0.1% (absolute) for samples 1–3 and $\sim$0.5% (absolute) for sample 4.

III. RESULTS AND DISCUSSION

Fig. 2(b) and (d) shows that the light I–V of the self-doped devices has a steep decrease ($\sim$ 0–0.5 V) in photocurrent much

TABLE I
MODEL PARAMETERS OF (5)–(7) EXPRESSED IN TERMS OF THE PHYSICAL PARAMETERS OF THE CELL

Variables	p-i-n / n-i-p	p-p-n	n-p-p
$1/\alpha_f$	$\dfrac{e^{V'} - 1}{V'} + \beta_f$	$\Delta + \beta_f \ (V \le V_{bi})$	$\Delta \times e^{V'} + \beta_f \ (V \le V_{bi})$
		$\dfrac{e^{V'} - 1}{V'} + \beta_f \ (V > V_{bi})$	
$1/\alpha_b$	$\dfrac{e^{V'} - 1}{V'} + \beta_b$	$\Delta \times e^{V'} + \beta_b \ (V \le V_{bi})$	$\Delta + \beta_b \ (V \le V_{bi})$
		$\dfrac{e^{V'} - 1}{V'} + \beta_b \ (V > V_{bi})$	
A	$a_f \times \left(\dfrac{1 - e^{V'-m}}{V' - m} - \beta_f\right)$	$\alpha_f \times \left(\dfrac{1}{m}(e^{-m\times\Delta} - 1) - \beta_f\right)(V \le V_{bi})$	$\alpha_f \times \left(\dfrac{e^{V'}}{m}(e^{-m} - e^{m\times(\Delta-1)}) - \beta_f\right)(V \le V_{bi})$
		$a_f \times \left(\dfrac{1 - e^{V'-m}}{V' - m} - \beta_f\right)(V > V_{bi})$	
B	$a_b \times \left(\dfrac{1 - e^{V'+m}}{V' + m} - \beta_b\right)$	$\alpha_b \times \left(\dfrac{e^{V'}}{m}(e^{-m\times(\Delta-1)} - e^{m}) - \beta_b\right)(V \le V_{bi})$	$\alpha_b \times \left(\dfrac{1}{m}(1 - e^{m\times\Delta}) - \beta_b\right)(V \le V_{bi})$
		$a_b \times \left(\dfrac{1 - e^{V'+m}}{V' + m} - \beta_b\right)(V > V_{bi})$	

Here, $(V' = q(V - V_{bi})/kT; \beta_{f(b)} = D/(t_o \times s_{f(b)}); m = t_o/\lambda_{ave}; n = W_d(0V)/t_o; \Delta = 1 - n\sqrt{(V_{bi} - V)/V_{bi}}$. The meaning of the parameters has been discussed in the text.
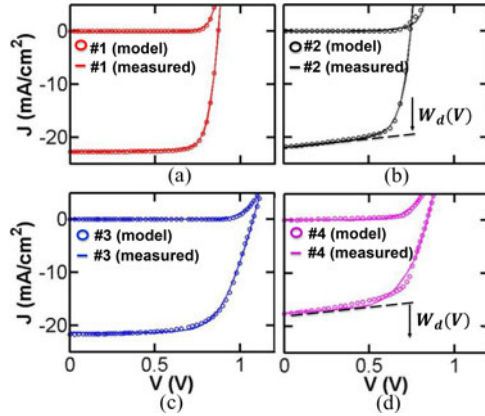

Fig. 2. (a) Samples #1 (Type-1 (p-i-n), efficiency = 15.7%, J_{SC} = 22.7 mA/cm^2, V_{OC} = 0.85 V, FF = 81%). (b) Samples #2 (Type-2 (p-p-n), efficiency = 11.1%, J_{SC} = 21.9 mA/cm^2, V_{OC} = 0.75 V, FF = 64%). (c) Samples #3 (Type-3 (n-i-p), efficiency = 15.4%, J_{SC} = 21.5 mA/cm^2, V_{OC} = 1.07 V, FF = 67%). (d) Samples #4 (Type-4 (n-p-p), efficiency = 8.6%, J_{SC} = 17.6 mA/cm^2, V_{OC} = 0.84 V, FF = 58%). Note that1) G_{max} = 23 mA/cm^2 is used. 2) Negligible parasitic resistors (R_{series} and R_{shunt}) except in samples #4.

TABLE II
EXTRACTED PHYSICAL PARAMETERS OF SAMPLES #1 [SEE FIG. 2(a)], #2 [SEE FIG. 2(b)], #3 [SEE FIG. 2(c)], AND #4 [SEE FIG. 2(d)]

Sample	#1	#2	#3	#4
Type	p-i-n	p-p-n	n-i-p	n-p-p
t_o (nm)	450	400	310	147
J_{f0} (mA/cm^2)	2.7×10^{-13}	4×10^{-12}	1.6×10^{-17}	6×10^{-15}
J_{b0} (mA/cm^2)	4×10^{-13}	5×10^{-13}	4.8×10^{-17}	4.1×10^{-13}
V_{bi} (V)	0.78	0.67	1	0.75
s_f (cm/s)	2×10^2	5×10^2	1×10^4	13.1
s_b (cm/s)	19.2	8.6×10^2	5.4	∞
$W_{depletion}$ (0V)(nm)	/	300	/	146

before the maximum power point (MPP). Indeed, this characteristic feature can be correlated with self-doping effects arising from the defects or impurities introduced during the manufacture of the cell. Our model interprets this linear decrease in photocurrent of type-2 and type-4 cells to the well-known voltage-dependent reduction of $W_d(V)$ (also the charge collection region) of a p-n junction. Without a physics-based model, this feature can be easily mistaken as a parasitic resistance. The self-doped devices also have an inferior V_{bi} and greater $J_{f0(b0)}$ that leads to a lower V_{OC}, compared with the intrinsic cells with the same configuration (see Table II). Hence, the main factor that limits the performance of samples #2 and #4 is the reduction of charge collection efficiency due to self-doping effect.

While examining the intrinsic samples #1 and #3, we note that #1 has the highest fill-factor (FF), but its V_{OC} is 0.3 V smaller than that of #3. The reduction in V_{oc} can be explained by lower V_{bi} and higher $J_{f0(b0)}$ caused by the combination of band misalignment and lower doping concentration in the transport layers of the perovskite cells with the traditional structure, which is the major performance limitation of #1. Sample #3, on the other hand, has the lower FF, arising from relatively high effective surface recombination velocities at both contacts, indicating insufficient blocking of charge loss to the wrong contact. Even though #1 and #3 have similar efficiencies, our model demonstrates that the fundamental performance limitations are completely different.

Using the model, we can also extract the thicknesses of the four samples, which are in the expected range ($\sim$350–500 nm for ##1 and #3, $\sim$330 nm for #2) [21], [31]. Among the samples, there is also a strong correlation between the absorber thickness t_0 and J_{SC} related to the completeness of the absorption. Moreover, we observe significant shunt resistance ($R_{shunt} = 1\,k\Omega \cdot cm^2$) in sample #4, which agrees with the reports [31] that thin absorber might lead to shunting pinholes. Further, except for sample #4, all devices have relatively poor (high) s_{front}, which may be caused by insufficient barrier
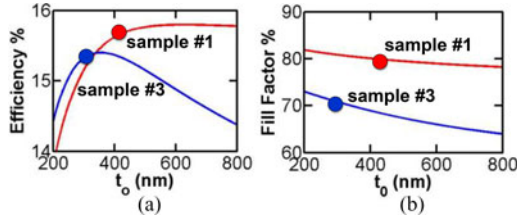
Fig. 3. (a) Efficiency versus absorber thickness for samples #1 and #3. (b) Fill factor versus absorber thickness for samples #1 and #3.
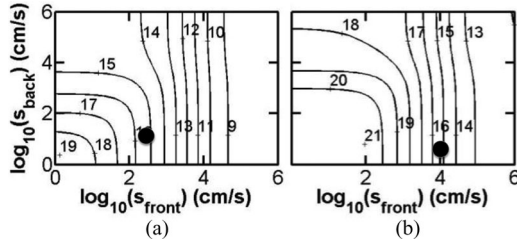

Fig. 4. (a) Contour plot of the front/back surface recombination velocities versus efficiency for sample #1. (b) Contour plot of the front/back surface recombination velocities versus efficiency for sample #3.

between PEDOT:PSS and perovskites [21], as well as poor carrier collection in TiO$_2$ [32]–[34].

Once we extract the physical parameters associated with high-efficiency samples (#1 and #3) with essentially intrinsic absorbers, it is natural to ask if the efficiency could be improved further, and if so, what factors would be most important. The physics-based compact model allows us to explore the phase-space of efficiency as a function of various parameters, as follows.

For example, while keeping all other parameter equal to the values extracted in Table II, one can explore the importance of absorber thickness on cell efficiency (see Fig. 3). Our model shows that both samples are close to their optimal thickness, although there is incomplete absorption ($J_{SC} < qG_{max}$). Thinner absorber cannot absorb light completely, while thicker absorber suppresses charge collection and degrades the fill factor. This is because the competition between the surface recombination and the electric field determines the carrier collection efficiency near the interface, and electric field $E = (V_{bi} - V)/t_o$ decreases with the thickness. To summarize, for the samples considered, thickness optimization would not improve performance.

Similarly, we can investigate the effects of the front/back surface recombination velocities on device efficiencies, with all other parameters kept fixed to those in Table II. The deduced surface recombination velocities for samples #1 and #3 are listed in Table II as well as labeled as black dots in Fig. 4. The results suggests that, in principle, improving the front surface recombination velocities by two orders of magnitude can boost the efficiency by ~3% and even ~5% for samples #1 and #3, respectively. Any potential improvement in the back selective blocking layer, however, offers very little gain, since most of the photogeneration occurs close to the front contact. Hence, engineering the front transport layer would be essential in further improvement of cell efficiencies.

However, even with the optimal surface recombination velocities, we are still not close to the thermodynamic limit (~30%) (see Fig. 4). Toward this goal, one must improve the J_{SC}, FF, and V_{OC} (thermodynamic limit: $J_{SC} \sim 26$ mA/cm^2, FF ~90%, $V_{OC} \sim 1.3$ V [35]). One may reduce the parasitic absorption loss in the transport layers, which can increase G_{max} in (4), to improve the J_{SC}; one may still improve the FF by increasing the charge diffusion coefficient D, since it is mainly the variable $\beta_{f(b)} = D/(t_o \times s_{f(b)})$ that determines the FF; one may also increase the built-in potential V_{bi}, through adjusting the band alignment at the interface as well as increasing the doping of the transport layers, to improve the V_{OC}.

We conclude this section with a discussion regarding hysteresis of the J–V characteristics, which can be an important concern for the inverted structure shown in Fig. 1(c) and (d). The phenomenon arises primarily from by trapping/detrapping of defects within the oxide or at the oxide/perovskite interface [32], [33]. Reassuringly, recent results show that process improvements, such as Li-treatment of TiO$_2$, can suppress/eliminate hysteresis (see [36]). Moreover, cells with the traditional structures [oxide-free, as in Fig. 1(a) and (b)] show very little hysteresis [21], [37]. Given the fact that hysteresis effects will be eventually minimized once perovskites are mature enough for integration in modules, the compact model proposed in this paper does not account for the effect of hysteresis explicitly.

IV. CONCLUSION

We have derived an analytical model that describes both dark and light current–voltage characteristics for four different types [p-i-n/p-p-n and n-i-p/n-p-p] of perovskite solar cells. An important contribution of the model is that, along with other measurement techniques, it provides a simple and complementary approach to characterize, optimize, and screen fabricated cells. Physical parameters that cannot be directly measured, such as V_{bi} of a p-i-n device, can also be deduced using the model.

Apart from determining the parameters of an existing cell and suggesting opportunities for further improvement, an analytical compact model serves another fundamental need, namely, the ability to predict the ultimate performance of the panel composed of individual perovskite cells. Panel efficiency is ultimately dictated by process variation reflected in various parameters (as in Table II), as well as statistical distribution of shunt and series resistances [13], [38]. Indeed, recent studies [39], [40] show large efficiency gap between perovskite-based solar cells and modules—an equivalent circuit based on the physics-based analytical model developed in this paper will be able to trace the cell-module efficiency gap to statistical distribution of one or more cell parameters and suggest opportunities for improvement. Closing this cell-to-module gap is the obvious next step and an essential prerequisite for eventual commercial viability of the perovskite solar cells.

APPENDIX

The parameters of the compact model are extracted by fitting the equations to experimental data. The fitting algorithm has two parts: 1) model choice and 2) iterative fitting.

Before one fits the data, the structure of the cell must be known (e.g., PEDOT:PSS/Perovskite/PCBM or TiO$_2$/Perovskite/Spiro-OMeTAD) and whether the absorber is self-doped or not. Ideally, the capacitance–voltage measurement provides the doping profile; as an alternative, we find that the steepness (*dI/dV*) of the light *I–V* curve at low voltage can also differentiate self-doped and intrinsic cells (see Fig. 2). Specifically, the light *I–V* of the self-doped device (sample #2) shows a steep decrease ($\sim$ 0–0.5 V) in photocurrent much before the MPP; an undoped device (sample #1), however, shows flat light *I–V* before MPP. If the parasitic resistance extracted from dark *I–V* is not significant, our model attributes this decrease in photocurrent to voltage-dependent reduction of the depletion region (charge collection) of a doped absorber. Such a feature helps one to choose the correct model for a device.

Estimating the initial guesses and limiting the range of each parameter (from physical considerations) is an important step, since the fitting procedure utilizes the iterative fitting function "lsqcurvefit" in MATLAB, whose results depend on the initial guesses significantly.

The physical parameters we attempt to deduce are $G_{\max}$, λ_{ave}, t_o, $W_d(0\text{V})$ (self-doped), D, s_f, s_b, V_{bi}, J_{f0}, and J_{b0}. Among these parameters, based on the transfer matrix method, $qG_{\max}$ can be obtained by integrating the photon absorption (around 23 mA/cm^2) and λ_{ave} is around 100 nm; $D \approx 0.05\,\text{cm}^2\text{s}^{-1}$ is known for the material system for both electrons and holes.

Presuming the dark current is illumination independent, one can calculate photocurrent following

$$J_{\text{photo}}\left(G, V\right) = J_{\text{light}}\left(G, V\right) - J_{\text{dark}}\left(V\right). \qquad (A1)$$

Since the absorber thickness is around 300–500 nm for perovskite solar cells, 400 nm is a sensible initial guess for t_o. Although capacitance measurement can determine $W_d(0\text{V})$ for a self-doped device, one can make $W_d\left(0\text{V}\right) \approx 300$ nm as an initial guess. It has been shown that s_f is inferior to s_b in most cases due to low insufficient barrier between PEDOT:PSS and perovskites as well as low carrier lifetime in TiO$_2$. Hence, the initial guesses for s_f and s_b could be approximately 10^3 and 10^2 cm/s, respectively. The junction built-in V_{bi} is estimated to be the crossover voltage of dark and light *I–V* curves. Then, one can first use the "lsqcurvefit" function to fit the photocurrent based on the initial guesses.

Since J_{f0} and J_{b0} is on the order of 10^{-13}–10^{-15} mA/cm^2, one can use zero as the initial guesses. Afterward, one can use the iterative fitting procedure for the dark current, while the parameters extracted from photocurrent are fixed.

Once the parameters are obtained, they must be checked for self-consistency and convergence between light and dark characteristics.

Acknowledgment

References

[1] S. Kazim, M. K. Nazeeruddin, M. Grätzel, and S. Ahmad, "Perovskite as light harvester: A game changer in photovoltaics," *Angew. Chem. Int. Ed. Engl.*, vol. 53, no. 11, pp. 2812–2824, Mar. 2014.

[2] M. A. Green, A. Ho-Baillie, and H. J. Snaith, "The emergence of perovskite solar cells," *Nat. Photon.*, vol. 8, no. 7, pp. 506–514, Jun. 2014.

[3] R. F. Service, "Energy technology. Perovskite solar cells keep on surging," *Science*, vol. 344, no. 6183, p. 458, May 2014.

[4] T. Minemoto and M. Murata, "Impact of work function of back contact of perovskite solar cells without hole transport material analyzed by device simulation," *Curr. Appl. Phys.*, vol. 14, no. 11, pp. 1428–1433, Nov. 2014.

[5] F. De Angelis, "Modeling materials and processes in hybrid/organic photovoltaics: From dye-sensitized to Perovskite solar cells," *Acc. Chem. Res.*, vol. 47, pp. 3349–3360.

[6] T. Minemoto and M. Murata, "Theoretical analysis on effect of band offsets in perovskite solar cells," *Sol. Energy Mater. Sol. Cells*, vol. 133, pp. 8–14, Feb. 2015.

[7] B. Tripathi *et al.*, "Temperature induced structural, electrical and optical changes in solution processed perovskite material: Application in photovoltaics," *Sol. Energy Mater. Sol. Cells*, vol. 132, pp. 615–622, Jan. 2015.

[8] J. M. Foster, H. J. Snaith, T. Leijtens, and G. Richardson, "A model for the operation of perovskite based hybrid solar cells: formulation, analysis and comparison to experiment," *SIAM J. Appl. Math.*, vol. 74, no. 6, pp. 1935–1966, 2014.

[9] W. W. Gärtner, "Depletion-layer photoeffects in semiconductors," *Phys. Rev.*, vol. 116, pp. 84–87, 1959.

[10] X. X. Liu and J. R. Sites, "Solar-cell collection efficiency and its variation with voltage," *J. Appl. Phys.*, vol. 75, no. 1, p. 577, Jan. 1994.

[11] S. Hegedus, D. Desai, and C. Thompson, "Voltage dependent photocurrent collection in CdTe/CdS solar cells," *Prog. Photovoltaics Res. Appl.*, vol. 15, no. 7, pp. 587–602, Nov. 2007.

[12] R. S. Crandall, "Modeling of thin film solar cells: Uniform field approximation," *J. Appl. Phys.*, vol. 54, no. 12, p. 7176, 1983.

[13] S. Dongaonkar and M. A. Alam, "End to end modeling for variability and reliability analysis of thin film photovoltaics," in *Proc. IEEE Int. Rel. Phys. Symp. Proc.*, 2012, pp. 4A.4.1–4A.4.6.

[14] S. S. Hegedus, "Current-voltage analysis of a-Si and a-SiGe solar cells including voltage-dependent photocurrent collection," *Prog. Photovoltaics*, vol. 5, no. 3, pp. 151–168, 1997.

[15] M. Hejri, H. Mokhtari, M. R. Azizian, M. Ghandhari, and L. Soder, "On the parameter extraction of a five-parameter double-diode model of photovoltaic cells and modules," *IEEE J. Photovoltaics*, vol. 4, no. 3, pp. 915–923, May 2014.

[16] K. Ishaque, Z. Salam, and H. Taheri, "Simple, fast and accurate two-diode model for photovoltaic modules," *Sol. Energy Mater. Sol. Cells*, vol. 95, no. 2, pp. 586–594, 2011.

[17] S. Dongaonkar, C. Deline, and M. A. Alam, "Performance and reliability implications of two-dimensional shading in monolithic thin-film photovoltaic modules," *IEEE J. Photovoltaics*, vol. 3, no. 4, pp. 1367–1375, Oct. 2013.

[18] K. Brecl and M. Topič, "Simulation of losses in thin-film silicon modules for different configurations and front contacts," *Prog. Photovoltaics Res. Appl.*, vol. 16, no. 6, pp. 479–488, 2008.

[19] K. Brecl, M. Topič, and F. Smole, "A detailed study of monolithic contacts and electrical losses in a large-area thin-film module," *Prog. Photovoltaics Res. Appl.*, vol. 13, no. 4, pp. 297–310, Jun. 2005.

[20] G. T. Koishiyev and J. R. Sites, "Impact of sheet resistance on 2-D modeling of thin-film solar cells," *Sol. Energy Mater. Sol. Cells*, vol. 93, no. 3, pp. 350–354, Mar. 2009.

[21] W. Nie *et al.*, "High-efficiency solution-processed perovskite solar cells with millimeter-scale grains," *Science*, vol. 347, no. 6221, pp. 522–525, Jan. 2015.

[22] A. Guerrero, E. J. Juarez-Perez, J. Bisquert, I. Mora-Sero, and G. Garcia-Belmonte, "Electrical field profile and doping in planar lead halide perovskite solar cells," *Appl. Phys. Lett.*, vol. 105, no. 13, p. 133902, Sep. 2014.

[23] V. D'Innocenzo *et al.*, "Excitons versus free charges in organo-lead trihalide perovskites," *Nat. Commun.*, vol. 5, no. 3586, 2014.

[24] M. M. Lee, J. Teuscher, T. Miyasaka, T. N. Murakami, and H. J. Snaith, "Efficient hybrid solar cells based on meso-superstructured organometal halide perovskites," *Science*, vol. 338, no. 6107, pp. 643–647, Nov. 2012.

[25] Q. Dong *et al.*, "Electron-hole diffusion lengths >175 m in solution grown $CH_3NH_3PbI_3$ single crystals," *Science*, vol. 347, no. 6225, pp. 967–970, Feb. 2015.

[26] S. D. Stranks *et al.*, "Electron-hole diffusion lengths exceeding 1 micrometer in an organometal trihalide perovskite absorber," *Science*, vol. 342, no. 6156, pp. 341–344, Oct. 2013.

[27] V. Gonzalez-Pedro *et al.*, "General working principles of $CH_3NH_3PbX_3$ perovskite solar cells," *Nano Lett.*, vol. 14, no. 2, pp. 888–893, Mar. 2014.

[28] L. A. Pettersson, L. S. Roman, O. Inganäs, and O. Inganäs, "Modeling photocurrent action spectra of photovoltaic devices based on organic thin films," *J. Appl. Phys.*, vol. 86, no. 1, p. 487, 1999.

[29] J. E. Moore *et al.*, "Correlation of built-in potential and I–V crossover in thin-film solar cells," *IEEE J. Photovoltaics*, vol. 4, no. 4, pp. 1138–1148, Jul. 2014.

[30] J. L. G. R. V. K. Chavali, J. E. Moore, X. Wang, M. A. Alam, and M. S. Lundstrom, "Frozen potential approach to separate the photo-current and diode injection current in solar cells," *IEEE J. Photovoltaics*, vol. 5, no. 3, pp. 865–873, May 2015.

[31] M. Liu, M. B. Johnston, and H. J. Snaith, "Efficient planar heterojunction perovskite solar cells by vapour deposition.," *Nature*, vol. 501, no. 7467, pp. 395–398, Sep. 2013.

[32] E. L. Unger *et al.*, "Hysteresis and transient behavior in current-voltage measurements of hybrid-perovskite absorber solar cells," *Energy Environ. Sci.*, vol. 7, pp. 3690–3698, 2014.

[33] H. J. Snaith *et al.*, "Anomalous hysteresis in perovskite solar cells," *J. Phys. Chem. Lett.*, vol. 5, no. 9, pp. 1511–1515, 2014.

[34] Y. Zhao and K. Zhu, "Charge transport and recombination in perovskite (CH3NH3)PbI3 sensitized TiO2 solar cells," *J. Phys. Chem. Lett.*, vol. 4, no. 17, pp. 2880–2884, Sep. 2013.

[35] M. A. Alam and M. Ryyan Khan, "Fundamentals of PV efficiency interpreted by a two-level model," *Am. J. Phys.*, vol. 81, no. 9, p. 655, Sep. 2013.

[36] J. Hyuck Heo *et al.*, "Hysteresis-less mesoscopic CH3NH3PbI3 perovskite Hybrid solar cells by introduction of Li-treated TiO2 electrode," *Nano Energy*, vol. 15, pp. 530–539, 2015.

[37] O. Malinkiewicz *et al.*, "Metal-oxide-free methylammonium lead iodide perovskite-based solar cells: The influence of organic charge transport layers," *Adv. Energy Mater.*, vol. 4, pp. 1–9, 2014.

[38] S. Dongaonkar *et al.*, "Universal statistics of parasitic shunt formation in solar cells, and its implications for cell to module efficiency gap," *Energy Environ. Sci.*, vol. 6, no. 3, pp. 782–787, 2013.

[39] F. Di Giacomo *et al.*, "Flexible perovskite photovoltaic modules and solar cells based on atomic layer deposited compact layers and UV-irradiated TiO_2 scaffolds on plastic substrates," *Adv. Energy Mater.*, vol. 5, 2015.

[40] F. Matteocci *et al.*, "High efficiency photovoltaic module based on mesoscopic organometal halide perovskite," *Prog. Photovoltaics Res. Appl.*, vol. 20, no. 1, pp. 6–11, 2014.

Wanyi Nie received the Ph.D. degree from the Department of Physics, Wake Forest University, Winston-Salem, NC, USA.

She is currently conducting research as a Postdoctoral Fellow with Los Alamos National Laboratory, Los Alamos, NM, USA, on optoelectronic device research with the Material Synthesis and Integrated Device Group, MPA-11. Her research interests include photovoltaic device physics and interface engineering.

Aditya D. Mohite received the B.S. and M.S. degrees from in solid-state physics from the Maharaja Sayajirao University of Baroda, Vadodara, India, and the Ph.D. degree from the University of Louisville, Louisville, KY, USA, in 2008, all in electrical engineering.

He is currently a Staff Scientist with the Materials Synthesis and Integrated Devices Group, Los Alamos National Laboratory, Los Alamos, NM, USA, where he directs an optoelectronics group (light to energy team) working on understanding and controlling photophysical processes in materials for thin-film light-to-energy conversion technologies such as photovoltaics, photocatalysis, etc. He is an expert with correlated techniques such as photocurrent microscopy and optical spectroscopy to investigate the charge and energy transfer and recombination processes in thin-film devices.

Xingshu Sun (S'13) received the B.S. degree from Purdue University, West Lafayette, IN, USA, in 2012, where he is currently working toward the Ph.D. degree in electrical and computer engineering.

His current research interests include device simulation and compact modeling for photovoltaics and nanoscale transistors.

Reza Asadpour received the B.Sc. and M.Sc. degrees in electrical engineering from University of Tehran, Tehran, Iran, in 2010 and 2013, respectively. Since 2013, he has been working toward the Ph.D. degree on solar cells and their reliability issues with Prof. Alam's CEED Group, Purdue University, West Lafayette, IN, USA.

Muhammad Ashraful Alam (M'96–SM'01–F'06) received the B.S.E.E. degree from the Bangladesh University of Engineering and Technology, Dhaka, Bangladesh, in 1988; the M.S. degree from Clarkson University, Potsdam, NY, USA, in 1991; and the Ph.D. degree from Purdue University, West Lafayette, IN, USA, in 1994, all in electrical engineering.

He is the Jai N. Gupta Professor of Electrical and Computer Engineering where his research and teaching focus on physics, simulation, characterization and technology of classical and emerging electronic devices. He received the B.S.E.E. degree from the Bangladesh University of Engineering and Technology, Dhaka, Bangladesh, in 1988, the M.S. degree from Clarkson University, Potsdam, NY, USA, in 1991, and the Ph.D. degree from Purdue University, West Lafayette, IN, USA, in 1994, all in electrical engineering. From 1995 to 2003, he was with Bell Laboratories, Murray Hill, NJ, where he made important contributions to reliability physics of electronic devices, MOCVD crystal growth, and performance limits of semiconductor lasers. At Purdue, Alam..s research has broadened to include flexible electronics, solar cells, and nanobiosensors.

Prof. Alam is a fellow of the AAAS, IEEE, and APS and recipient of the 2006 IEEE Kiyo Tomiyasu Award for contributions to device technology.